

Generalization of Kuramoto model in vector product form

Hyun Keun Lee¹ and Hyunsuk Hong^{2,*}

¹*Department of Physics, Sungkyunkwan University, Suwon 16419, Korea*

²*Department of Physics and Research Institute of Physics and Chemistry,
Jeonbuk National University, Jeonju 54896, Korea*

(Dated: August 16, 2022)

We generalize the Kuramoto model of coupled phase oscillators in 3-dimensional space, via a vector product form. It is demonstrated that the standard Kuramoto model can be transformed to a vector product form. This form gives the generalized model as the phase and the natural frequency of oscillator are, respectively, represented by position on unit sphere and 3-dimensional frequency vector. The long-term collective states are illustrated, which are arguable with the geometric intuition motivated by the model structure, the vector product form. Our prediction shows a good consistency with numerical observations. We illustrate the conventional numerical integration method for the Kuramoto model in 3-dimension is accompanied by unavoidable ambiguity, and show this problem is resolved in the new method direct from our model equation.

PACS numbers: 05.45.-a, 89.65.-s

I. INTRODUCTION

Kuramoto model [1] is one of the prototypes for the study of the synchronization phenomena frequently observed in nature [2–4]. It is a mathematical model for describing the collective behavior in the population of coupled oscillators. The model is composed of the coupling terms depicting the interaction among the phase oscillators and the natural frequencies randomly distributed according to a distribution function such as Gaussian or Lorentzian one. When the coupling is strong enough to overcome the diversity of the natural frequencies, synchronization appears. Variants of the Kuramoto model have been suggested from the aspect of time delay [5], inertia effect [6, 7], presence of noise [8], and so forth, which is basically a reflection of reality or a generalization of the Kuramoto model. Coupled oscillator models have provided frameworks in the theoretical and practical study of swarming [9–14] or flocking [15, 16] behavior of natural and artificial systems.

One of the interests in the generalizations of the Kuramoto model is to increase the dimension of the phase variable, equivalently, that of the embedding space. The pioneering work in this direction is the consensus models where individual's opinion is represented by vector in general [17]. Later, it is reported that the generalization can be direct from the algebra of rotation group theory [18–21]. After equipped with this algebraic tool, Kuramoto model in higher dimension has been steadily studied [22–28]. In those studies, the theoretical predictions and numerical data are usually illustrated in 3-dimensional space, above which a sensible visualization is not allowed. The geometrical sense or intuition in 3-dimension plays the non-replaceable role in examining the results. Therefore, a solid description and understanding on the model in 3-dimension is necessary.

In the present paper, we report that there is another route to the generalization of the Kuramoto model to 3-dimension. We demonstrate that the standard Kuramoto model can be understood with a vector product form composed of the positions on unit sphere and 3-dimensional natural frequency vectors. The original Kuramoto model is recovered when initial position and natural frequency are properly chosen. We survey a few long-term states predictable through the model structure, the vector product form. This theoretical understanding is supported by numerical observations. It is finally illustrated that the model equation we have recognized this time directly gives a new numerical integration method free from such ambiguity that is inevitable in the conventional numerical method.

This paper is organized as follows. In Sec. II, our generalization of the Kuramoto model to 3-dimension is presented. Two extreme features of the model are shown in Sec. III, and this is used for the understanding of the long-term states of the model in Sec. IV. The new numerical method by our model equation is explained in Sec. V. This work finishes in Sec. VI with a brief summary.

II. GENERALIZATION OF KURAMOTO MODEL

The Kuramoto model is given by a differential equation for the dynamics of coupled phase oscillators:

$$\dot{\theta}_i = \omega_i + \frac{K}{N} \sum_{j=1}^N \sin(\theta_j - \theta_i), \quad (1)$$

where $\theta_i \in [0, 2\pi)$ is the phase of oscillator i and ω_i is its natural frequency. The $K > 0$ represents the coupling constant and N is the number of oscillators in the system.

We consider a circle of unit radius at the origin of x - y plane in 3-dimensional space. Then, in Cartesian coordinate system, we introduce the position vector for os-

* Corresponding author: hhong@jbnu.ac.kr

oscillator i of phase θ_i on the circle: $\mathbf{r}_i = (x_i, y_i, 0) = (\cos \theta_i, \sin \theta_i, 0)$. This way, the oscillator of phase θ_i can be also identified with a particle or an agent at position \mathbf{r}_i . Below, for convenience, we interchangeably use oscillator, particle, or agent. Similarly, for oscillator j , it reads that $\mathbf{r}_j = (\cos \theta_j, \sin \theta_j, 0)$. For \mathbf{r}_i and \mathbf{r}_j written this way, one can observe that i) $\dot{\mathbf{r}}_i = (-\sin \theta_i, \cos \theta_i, 0)\dot{\theta}_i$, ii) $\mathbf{w}_i \times \mathbf{r}_i = (-\sin \theta_i, \cos \theta_i, 0)\omega_i$ for $\mathbf{w}_i = (0, 0, \omega_i)$ and vector product operator \times [21], and iii) $(\mathbf{r}_i \times \mathbf{r}_j) \times \mathbf{r}_i = (-\sin \theta_i, \cos \theta_i, 0)\sin(\theta_j - \theta_i)$.

These observations lead us to convert Eq. (1) in a vector product form given by

$$\dot{\mathbf{r}}_i = \mathbf{w}_i \times \mathbf{r}_i + \frac{K}{N} \sum_{j=1}^N (\mathbf{r}_i \times \mathbf{r}_j) \times \mathbf{r}_i. \quad (2)$$

This formula is straightforwardly derived in use of the observations listed above after applying $(-\sin \theta_i, \cos \theta_i, 0)$ on both sides of Eq. (1). Equation (2) is the spatial-coordinate representation of the standard Kuramoto model in Eq. (1) when subject to the restriction of $\mathbf{r}_i = (\cos \theta_i, \sin \theta_i, 0)$ and $\mathbf{w}_i = (0, 0, \omega_i)$.

For a compact expression of Eq. (2), we introduce $\mathbf{k} \equiv K \sum_j \mathbf{r}_j / N = K \mathbf{r}_{\text{CM}}$, where \mathbf{r}_{CM} is the position center of the agents in the system. For this \mathbf{k} , Eq. (2) is simply rewritten as

$$\dot{\mathbf{r}}_i = (\mathbf{w}_i - \mathbf{k} \times \mathbf{r}_i) \times \mathbf{r}_i. \quad (3)$$

The minus sign on the right hand side of Eq. (3) comes from $\mathbf{r}_i \times \mathbf{r}_j = -\mathbf{r}_j \times \mathbf{r}_i$. As a 3-dimensional vector equation, Eq. (3) is the generalized Kuramoto model, which we will study in this work. To explore the properties of Eq. (3) in the aspect of a generalized phase, we consider \mathbf{r}_i on the unit sphere centered at the origin, and use general $\mathbf{w}_i = (\omega_{i,x}, \omega_{i,y}, \omega_{i,z})$ that is not necessarily parallel to \mathbf{z} -axis.

Equation (3) is structured as $\dot{\mathbf{r}}_i = \mathbf{a} \times \mathbf{r}_i$ for a vector \mathbf{a} . Then, in the fact that $\dot{\mathbf{r}}_i \perp \mathbf{r}_i$, \mathbf{r}_i resides forever on the unit sphere if initially provided that $\|\mathbf{r}_i(0)\| = 1$ for all i . This initial condition is also a part of the generalized Kuramoto model. We point out that $\|\mathbf{r}_i\| = 1$ for $t > 0$ is not a condition for the model equation Eq. (3) but a consequence from it equipped with the initial condition. Therefore, \mathbf{r}_i can be interpreted as spherical phase of agent i , and its differential equation Eq. (3) governs the dynamics of the spherical phase. We remark that Eq. (3) has its concrete meaning in 3-dimensional space where the vector product is well defined.

Since the vector product \times is a linear operation, one may consider a matrix W_i that satisfies $W_i \mathbf{r}_i = \mathbf{w}_i \times \mathbf{r}_i$. From the detail of the operation \times , it is given that

$$W_i = \begin{pmatrix} 0 & -\omega_{i,z} & \omega_{i,y} \\ \omega_{i,z} & 0 & -\omega_{i,x} \\ -\omega_{i,y} & \omega_{i,x} & 0 \end{pmatrix}. \quad (4)$$

Additionally, by the identity $\mathbf{a} \times (\mathbf{b} \times \mathbf{c}) = (\mathbf{a} \cdot \mathbf{c})\mathbf{b} - (\mathbf{a} \cdot \mathbf{b})\mathbf{c}$ [21], Eq. (3) is rewritten as

$$\dot{\mathbf{r}}_i = W_i \mathbf{r}_i + \mathbf{k} - (\mathbf{k} \cdot \mathbf{r}_i)\mathbf{r}_i. \quad (5)$$

We note that Eq. (5) is identical to the expression pioneered in Ref. [17] for $\mathbf{w}_i = 0$ and also to what formulated in Ref. [18, 23] for general \mathbf{w}_i .

As stated, our vector product form in Eq. (3) can be rewritten as the conventional one in Eq. (5). We however do not use this conventional one in the present work. Instead, we exploit the edges of the vector product form over the conventional equation in studying the long-term states of the Kuramoto model in 3-dimension. The vector product form we have recognized this time is expected to be an useful and intuitive tool from the geometrical point of view. In the following, it will be demonstrated that the vector product form plays the compact and neat role in the analytic and numerical study of the Kuramoto model in 3-dimension.

III. TWO EXTREME BEHAVIORS

We first consider the motion of the agents subject to the natural frequency part only. This is the case when $K = 0$ in Eq. (3). The equation of motion is then simply given by

$$\dot{\mathbf{r}}_i = \mathbf{w}_i \times \mathbf{r}_i = W_i \mathbf{r}_i. \quad (6)$$

Consider $\mathbf{u}_{i,3} = \mathbf{w}_i / \|\mathbf{w}_i\|$, and let $\mathbf{u}_{i,1}$ and $\mathbf{u}_{i,2}$ be the unit vectors chosen to satisfy $\mathbf{u}_{i,1} \times \mathbf{u}_{i,2} = \mathbf{u}_{i,3}$. Then, linear algebra gives the solution as

$$\mathbf{r}_i(t) = \mathbf{u}_{i,1} \rho_i \cos(\omega_i t + \phi_i) + \mathbf{u}_{i,2} \rho_i \sin(\omega_i t + \phi_i) + \mathbf{u}_{i,3} l_i, \quad (7)$$

where $\omega_i = \|\mathbf{w}_i\|$, $l_i = \mathbf{u}_{i,3} \cdot \mathbf{r}_i(0)$, $\rho_i = \sqrt{1 - l_i^2}$, and ϕ_i is a value determined by $\mathbf{r}_i(0)$ and the choice of $\mathbf{u}_{i,2}$. Equation (7) corresponds to a rotation on the surface of unit sphere, a limit cycle, at latitude l_i assigned along the $\mathbf{u}_{i,3}$ -axis. All decoupled oscillators by $K = 0$ display their own rotations on the surface. We call the behavior by Eq. (6) *spinning*.

On the other hand, when $\mathbf{w}_i = 0$ in Eq. (3) for all i , the dynamics is governed by

$$\dot{\mathbf{r}}_i = -(\mathbf{k} \times \mathbf{r}_i) \times \mathbf{r}_i. \quad (8)$$

For this nonlinear differential equation, one can expect the steady state with $\dot{\mathbf{r}}_i = 0$ for all i . By the structure of Eq. (8), the steady state is only accompanied with $\mathbf{k} \times \mathbf{r}_i = 0$. There are two possibilities: the system may approach to such configuration of $\mathbf{k} \propto \sum_j \mathbf{r}_j = 0$ or, otherwise, may form such \mathbf{k} that is parallel to \mathbf{r}_i . We consider that the first case is hard to have dynamic stability. Compared to this, the second case is natural because the positive coupling ($K > 0$) drives the agents get closer to the others, which readily achieves a complete gathering together. It is thus expected that $\mathbf{r}_i = \mathbf{r}_j$ for all i and j in the $t \rightarrow \infty$ limit. Such gathering behavior was studied in [17], and this was later called the synchronization in [23]. We also numerically observe the similar behavior as shown in Fig. 1. We call the close aggregation by Eq. (8) *converging*.

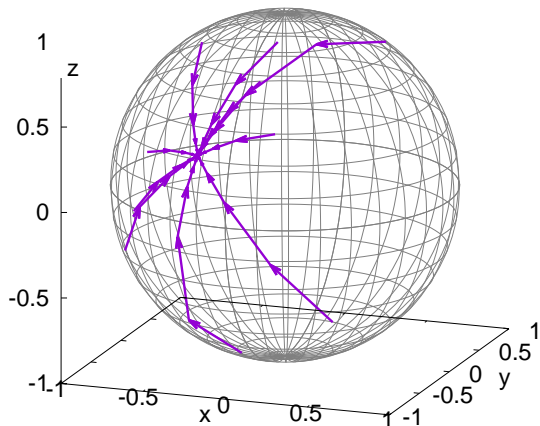


FIG. 1. (Color Online) Numerical observation of converging behavior by coupling term only. The destination that all the trajectories heading to is the fixed-point solution of Eq. (8). Each trajectory represents an agent's motion, and the arrow line is the displacement during unit time. For numerical integration, a new method by the model equation [Eq. (3)] is used instead of the conventional one (the new method applied through this work is explained in Sec. V). We use $\Delta t = 0.01$ for time-mesh and $K = 1$. Initially, the oscillators are randomly distributed on the surface of unit sphere following uniform distribution (the same initial condition is applied to all numerical calculations in this work). We show the trajectory in the system of $N = 10$ oscillators for clarity (see the movie “fig1-100.gif” for $N = 100$ in the supplementary material).

The two extreme behaviors mentioned above are, respectively, the limiting properties of the differential equation in Eq. (3). These provide basic understanding or predicting blocks of the long-term states expected for the generalized Kuramoto model in 3-dimension, as demonstrated below.

IV. LONG-TERM STATES

In this section, we examine a few long-term states of Eq. (3) where the term for spinning and that for converging play their roles simultaneously. For this, it is considered from now on that $K > 0$ and $\mathbf{w}_i \neq 0$ at least for an i . We restrict our interest to such states that are arguable with the geometrical meaning of the vector product and also with numerical data. For the arguable collective behaviors, we focus on the rather simple situation with $\|\mathbf{r}_{\text{CM}}\| \approx 1$ after initial transient period.

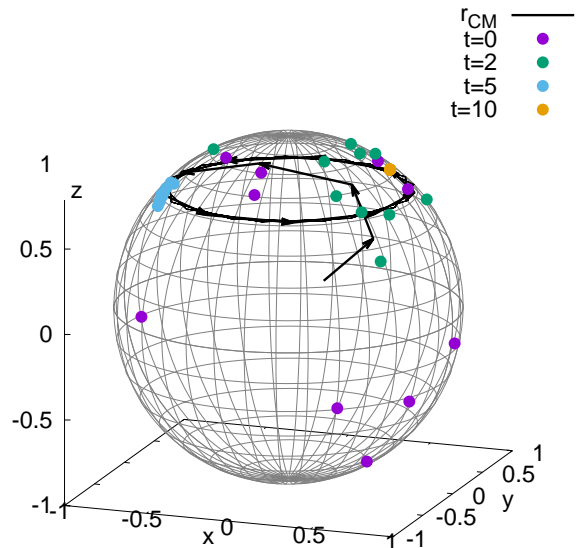


FIG. 2. (Color Online) Formation of the limit cycle of synchronized agents with $\mathbf{w}_i = \mathbf{w} (\neq 0)$ for all i . The solid circles with different color represent the agents at the specified time, and the black bold line with arrow is the trajectory of the position center of the agents. The arrow segment is the displacement of the position center for unit time. The sequence of the black bold line shows that the limit cycle is apparently formed around $t = 5$. We set $\|\mathbf{w}\| = 1$, $\Delta t = 0.01$, and $K = 1$. The z -axis is chosen as the direction of \mathbf{w} for simplicity. See also the movie “fig2-100.gif” for $N = 100$ in supplementary material.

A. Identical frequency ($\mathbf{w}_i = \mathbf{w}$)

We first consider the case of $\mathbf{w}_i = \mathbf{w}$ for all i . For this setting, what called the dynamical synchronization was reported as a long-term state [23], which is realized through a limit cycle of the clustered oscillators. In the present study, we also obtain similar numerical data as shown in Fig. 2. We understand it as the spinning of the sufficiently aggregated oscillators by the converging. First, all agents gather before long; the data points at $t = 10$ in Fig. 2, already, almost look like a single point (the deviation of all agents' locations is much smaller than the size of the point). Thereafter, $\mathbf{r}_i \approx \mathbf{r}_{\text{CM}}$ so that $\mathbf{k} \times \mathbf{r}_i \approx 0$. When these approximations are applied to Eq. (3), it follows that $\dot{\mathbf{r}}_{\text{CM}} \approx \mathbf{w} \times \mathbf{r}_{\text{CM}}$ whose structure is similar to that of Eq. (6). Then, \mathbf{r}_{CM} readily gives the limit cycle like Eq. (7). Since $\|\mathbf{r}_{\text{CM}}\| \rightarrow 1^-$, all agents form the almost fully synchronized state, and the resultant cluster rotates at a constant latitude assigned on the $\mathbf{w}/\|\mathbf{w}\|$ -axis. In analytic point of view, if considered in the rotating frame of angular velocity \mathbf{w} , the behavior is simply a converging like what shown in Fig. 1. Its

compact mathematical proof is given in [23].

The limit cycle for the dynamical synchronization was already predicted [18, 23] in the system of nonzero identical natural frequency vectors, and the supporting numerical data were also mentioned [18] or displayed [23]. However, contrary to the simple and convincing argument for the existence of such limit cycle, the numerical evidence was rather restricted. For example, a rather small system of $N \leq 10$ is suggested [18] or the numerical data of [23] is for $N = 4$. Compared to this, our numerical tests generate the dynamical synchronization independent of N . We consider that our reliable numerical realization is attributed to the new numerical method as a direct application of our model equation Eq. (3). This issue regarding the comparison between our numerical method and that used in the previous studies will be separately discussed below in Sec. V.

B. Parallel frequency ($\mathbf{w}_i \propto \mathbf{w}_j$)

The next case is that all \mathbf{w}_i s are not identical but parallel with each other, i.e., $\mathbf{w}_i \propto \mathbf{w}_j$ for all i and j . In this case, it seems that the oscillators do not show a converging behavior due to heterogeneous spinning strengths by the different magnitudes of \mathbf{w}_i s. In brief, different spinnings of agents may prevent their converging, and vice versa. We here note that there are two locations where the spinning and the converging do not contradict each other. The places are the poles, the two intersection points between the axis of spinning (this axis is unique because all \mathbf{w}_i s are parallel) and the surface of the sphere. This is because the spinning on the poles does not give any actual motion. Then, the conflict between spinning and converging will vanish as all the agents approach to one of the poles. If this takes place, the system finally shows the fixed point solution at the pole.

Figure 3 is the numerical observation where the trajectory of the position center finally forms a spiral to the fixed point (SFP). In early stage, a limit cycle seems to appear, but this arrives at a fixed point in the end. Although a cycle lasts longer for larger K and smaller N , it finally disappears in the numerical tests. The data obtained for $K = 32$ and $N = 10$ are shown in Fig. 3. As long as K is not infinite, no place except the poles can be the fixed point due to the conflict between spinning and converging. In the numerical simulations, we have not observed the other kind of long-term state except SFP for nonidentical parallel \mathbf{w}_i s.

A similar numerical observation was also reported in [18]. However, that was classified therein as a limit cycle in the mention that the parallel \mathbf{w}_i s is a necessary condition for the limit cycle. In contrast, we have not observed such limit cycle in the numerical simulations. We here indicate that necessary condition does not guarantee consequence. In our numerical tests, the ultimate feature is not the limit cycle but a fixed point regardless of the early stage patterns, and this is consistent with

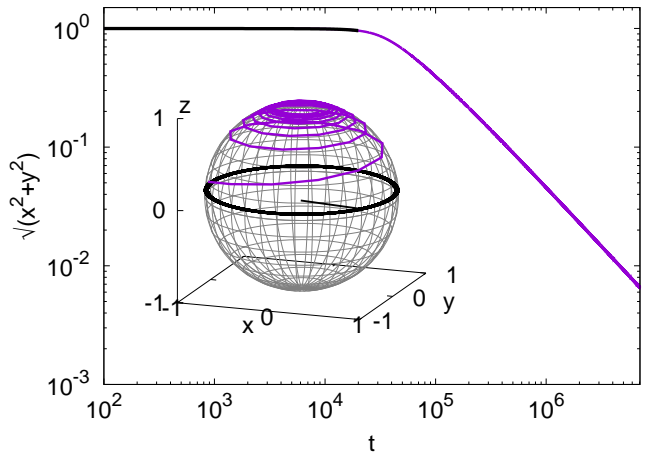


FIG. 3. (Color Online) SFP by non-identical parallel \mathbf{w}_i s. The vertical value of the main plot is the numerically obtained distance between the position center (x, y, z) at time t of the agents in the system and the rotation axis; z -axis is chosen as the direction of the rotation, i.e., $\mathbf{w}_i = \omega_i \mathbf{z}$. As shown, $\sqrt{x^2 + y^2}$ stays around 1 even up to $t \approx 10^4$ (the horizontal black line). However, it decays thereafter following $\rho \sim t^{-c}$ for a positive c (the declining purple line), where $c \approx 1$ by fitting the data. This asymptotic form is used in the inset to draw the spiral to the fixed point at the pole (the purple curve in the upper hemisphere). The black curve in the inset shows the trajectory up to $t \approx 10^4$. We use $\Delta t = 0.01$, $K = 32$, and $N = 10$. The ω_i are chosen from the uniform distribution with unit mean and the width 0.2.

our understanding on the role of pole as a fixed point solution. Although a seemingly limit cycle lasts for long time in some cases, its eventual shape is supposed to be a spiral to the fixed point at pole.

We add that our argument for the approach to the pole does not require a threshold of coupling strength. In our numerical analysis, spiral to the pole always shows up for various values of K . We thus conjecture that the spiral to the pole occurs for any $K > 0$. Because the pole as a fixed point is on the surface of the unit sphere, the order parameter of spatial synchronization approaches 1 following the spiral, i.e., $\|\mathbf{r}_{\text{CM}}\| \rightarrow 1^-$ as $t \rightarrow \infty$. The exception is only when all agents are initially at the equator determined by the pole. Remind that this initialization with parallel natural frequency recovers the standard Kuramoto model. Under this exceptional setup, a finite coupling-strength threshold is required for a synchronization as well-known for the standard Kuramoto model [1–4]. We here remark that synchronization on the equator needs a coupling-strength threshold to overcome the different spinnings, which is not the case for the synchronization at pole. We thereby consider that such finite threshold is not a generic property of synchronization for the 3-dimensional model in the sense that the initialization at equator only is measure zero out of the possible configurations on the unit sphere.

C. General frequency & strong coupling

For general \mathbf{w}_i s, it is not easy to predict the long-term behavior in an intuitive way. In order to see what happens in the system, we restrict our interest to the case of large K , by which a close gathering of oscillators is expected. When the oscillators are sufficiently close to the others, it reads that $\mathbf{r}_i \approx \mathbf{r}_{\text{CM}}$ for all i . Then, since \mathbf{k} is parallel to \mathbf{r}_{CM} by definition, it reads that $(\mathbf{k} \times \mathbf{r}_i) \times \mathbf{r}_i \approx 0$. When this is applied to Eq. (3), $\dot{\mathbf{r}}_i \approx \mathbf{w}_i \times \mathbf{r}_i$ seems to follow. However, this approximation is unacceptable as follows.

Most of all, ignoring $(\mathbf{k} \times \mathbf{r}_i) \times \mathbf{r}_i$ in Eq. (3) can be also caused by weak coupling with small K . Obviously, $\dot{\mathbf{r}}_i \approx \mathbf{w}_i \times \mathbf{r}_i$ is immediate from Eq. (3) for sufficiently small K . Note that the negligible coupling by $K \approx 0$ is opposite to the strong one by large K , and we are interested in the latter case. Therefore, if $(\mathbf{k} \times \mathbf{r}_i) \times \mathbf{r}_i$ is ignored by close gathering, the condition that the system is in the strong coupling regime of large K should be reflected somewhere in Eq. (3). Only $\mathbf{w}_i \times \mathbf{r}_i$ part that remains after ignoring $(\mathbf{k} \times \mathbf{r}_i) \times \mathbf{r}_i$ can provide a room for the reflection. We here suggest that, after initial transient period, \mathbf{w}_i could be simply replaced with an effective one $\mathbf{w}_{i,\text{eff}} = \alpha \mathbf{w}_i$ for a proper α . In the meantime, since we also expect $\mathbf{r}_i \approx \mathbf{r}_{\text{CM}}$ for large K , it follows that $\dot{\mathbf{r}}_i \approx \alpha \mathbf{w}_i \times \mathbf{r}_{\text{CM}}$ from Eq. (3). Taking its average over i leads to

$$\dot{\mathbf{r}}_{\text{CM}} \approx \alpha \mathbf{w}_m \times \mathbf{r}_{\text{CM}}, \quad (9)$$

where $\mathbf{w}_m \equiv \sum_i \mathbf{w}_i / N$ is the mean of the natural frequency vectors.

As the simple steady state of Eq. (9), one may expect the fixed point of \mathbf{r}_{CM} . When $\dot{\mathbf{r}}_{\text{CM}} = 0$ is considered at a fixed point \mathbf{r}_{CM}^* , $\|\mathbf{r}_{\text{CM}}^*\| \approx 1$ and $\mathbf{w}_{\text{eff}} \times \mathbf{r}_{\text{CM}} \approx 0$ gives

$$\mathbf{r}_{\text{CM}}^* \approx \pm \hat{\mathbf{w}}_m, \quad (10)$$

where $\hat{\mathbf{w}}_m \equiv \mathbf{w}_m / \|\mathbf{w}_m\|$. The fixed point \mathbf{r}_{CM}^* in Eq (10) covers what argued for the parallel \mathbf{w}_i s in Sec. IV B. An implication of Eq (10) is that the location of the fixed points, intuitively argued in Sec. IV B, can be generalized to the direction vector of the average of natural frequency vectors or its antipodal opposite (note that there is \pm sign in front of $\hat{\mathbf{w}}_m$). Accordingly, the SFP is also expected for general natural frequency when the coupling is strong enough. In Fig. 4, we display the numerical observation where a purple spiral, the trajectory of position center, heads to a red solid circle at $\mathbf{r}_{\text{CM}}^* = -\hat{\mathbf{w}}_m$ (see the upper hemisphere). This is the numerical evidence that the SFP, discussed in Sec. IV B for parallel \mathbf{w}_i , can be a rather general phenomenon.

As the other long-term state of Eq. (9), a limit cycle is possible. This is because the non-steady state solution like Eq. (7) can be expected (see Eq. (9) has the same structure as that of Eq. (6)). We numerically observe that the trajectory of the position center approaches to the limit cycle whose rotation axis is $\hat{\mathbf{w}}_m$. Interestingly, the targeted limit cycles are always the great circles in

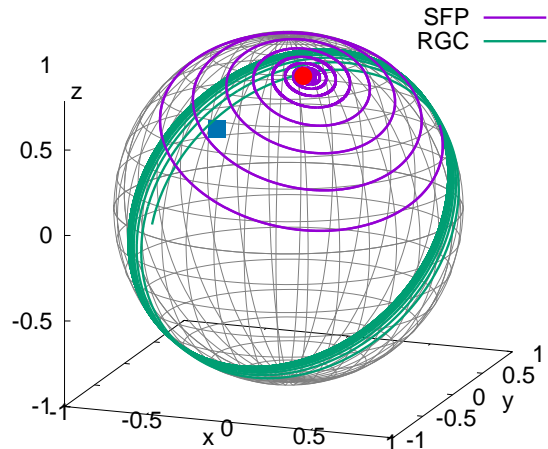


FIG. 4. (Color Online) Two types of long-term trajectories of position center for general \mathbf{w}_i . The purple curve in the upper hemisphere is SFP while the green one that also occupies the lower part is RGC. The red solid circle given by Eq. (10) is the destination of the SFP. The blue solid square on the back side of the sphere, given by $\hat{\mathbf{w}}_m$, is the pole for the associated equator to which the RGC approaches. We set $\Delta t = 0.01$, $K = 16$, and $N = 100$. The \mathbf{w}_i s are chosen from the distribution whose direction part is uniform for all solid angle and length part is also uniform with unit mean and unit width. Initial positions of the agents are chosen to be uniformly random. See also the movie “fig4-sfp.gif” and “fig4-rgc.gif” in supplementary material.

the numerical tests. So, the observed trajectory after initial period is the rotation approaching to great circle (RGC). An instance is the green curve that spans the upper and lower hemispheres in Fig. 4. Therein, the trajectory very close to the great circle gives $\alpha < 0.2$. Whether a system will show SFP or RGC depends on initial condition and natural frequency, respectively, randomly chosen from certain distributions (see the caption in Fig. 4 for the detail specification).

Although obtained in an arguable way, Eq. (9) captures a few interesting properties of the long-term states of Eq. (3), as illustrated. We expect that this approach and findings will provide a guide in the further study of the long-term solutions. For a background of the present study, a rigorous examination on the validity of Eq. (9) itself will be meaningful. In the meantime, different from Sec. IV B, a threshold of coupling strength seems necessary for the onset of the long-term states found here in Sec. IV C. Existence of such threshold is one of the interesting issues, and (if exists) exploring the states below

that will be also an interesting work.

V. NUMERICAL METHOD FOR ON-SPHERE SMOOTH MOTION

In the numerical study, $\mathbf{r}(t + \Delta t)$ is determined with $\mathbf{r} = \mathbf{r}(t)$ and $\dot{\mathbf{r}} = \dot{\mathbf{r}}(t)$ for a small time-mesh Δt (we below omit the index of agent for simplicity unless confusing). For a given $\Delta \mathbf{s} = \dot{\mathbf{r}}\Delta t$ at \mathbf{r} , exploiting the property $\Delta \mathbf{s} \perp \mathbf{r}$, the conventional method chooses the point where the position vector $\mathbf{r} + \Delta \mathbf{s}$ penetrates the unit sphere centered at origin as $\mathbf{r}(t + \Delta t)$. This is the method suggested in the seminal work [17]. At a glance, this method seems to have no ambiguity in choosing $\mathbf{r}(t + \Delta t)$ for the given $\Delta \mathbf{s}$. However, this is not the case, as will be explained below. Before going further, we remark that the numerical result in [17] is still valid because natural frequency is not taken into account therein. This point will also become clear in the following.

A. Instantaneous rotation

Smooth motion on sphere is a continuous patch of infinitesimal arcs of their own curvatures. Thus when $\Delta \mathbf{s}$ is given, numerical method should specify a circle on the sphere, which is tangential to $\Delta \mathbf{s}$. Then, $\mathbf{r}(t + \Delta t)$ is given by the intersection point between the circle and the line segment from the circle's center to the endpoint of the position vector $\mathbf{r} + \Delta \mathbf{s}$. Here, we emphasize that such circle is not unique, and thereby the position update becomes different depending on the circles.

In order to illustrate this point, we draw the purple and green circles in Fig. 5, which are tangential to the black bold arrow at the starting point (this arrow represents $\Delta \mathbf{s}$ and its starting point is \mathbf{r}). Since the green one is a great circle (see the caption), if position update is considered on it, this corresponds to the method in [17]. However, this is merely a choice replaceable with what by the purple circle on the upper hemisphere. There is no reason to prefer the green one to the purple circle. Furthermore, there can be infinite number of circles, each of which is tangential to the bold arrow at the same point. Figure 5 thereby implies that infinite number of choices are possible in numerically specifying the position update for given $\Delta \mathbf{s}$.

Therefore, any numerical method that updates the position with $\Delta \mathbf{s}$ only is basically incomplete. Thus, to obtain the proper displacement, one should specify the rotation axis that gives the circle along which the position update takes place. Our formula Eq. (3) has the advantage that it explicitly shows that axis. The rotation axis is no more than the direction vector of $\mathbf{v}_i \equiv (\mathbf{w}_i - \mathbf{k} \times \mathbf{r}_i)$, the leading factor of the right hand side of Eq. (3). This is because Eq. (3), we have formulated for model equation, is structured as $\dot{\mathbf{r}} = \boldsymbol{\Omega} \times \mathbf{r}$ that states a particle at \mathbf{r} rotates by angular velocity $\boldsymbol{\Omega}$ along the rotation axis

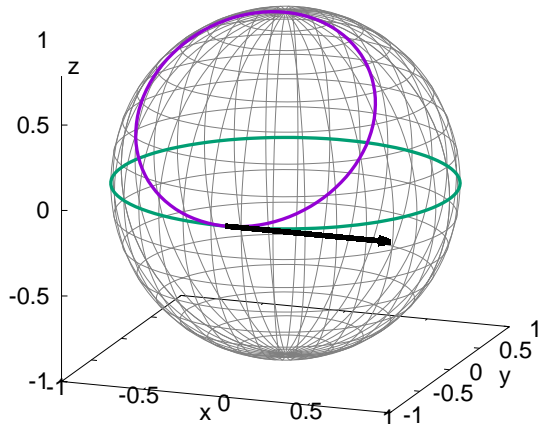


FIG. 5. (Color Online) A schematic for the ambiguity of rotation axis. The black bold arrow represents the tangential vector to the equator of green color. The purple circle turning around from the arctic pole is also tangential to the equator at the same point. When the black arrow is $\Delta \mathbf{s}$ (see the text), it is ambiguous whether the displacement should take place on either purple or green one. There are infinitely many circles that can play the similar role though we draw only two for simplicity.

$\boldsymbol{\Omega}/\|\boldsymbol{\Omega}\|$ [29]. Consequently, the rotation axis we are seeking for is $\hat{\mathbf{v}}_i = \mathbf{v}_i/\|\mathbf{v}_i\|$. We remark that this axis itself dynamically evolves in time because $\mathbf{v}_i = (\mathbf{w}_i - \mathbf{k} \times \mathbf{r}_i)$ is attributed to the set of dynamic variables $\{\mathbf{r}_i\}$.

B. Finite rotation as numerical integration

This way, $\dot{\mathbf{r}}_i = \mathbf{v}_i \times \mathbf{r}_i$ for $\mathbf{v}_i = (\mathbf{w}_i - \mathbf{k} \times \mathbf{r}_i)$ explicitly shows how the position update of agent i takes place. It is thus not necessary to use $\Delta \mathbf{s} (= \mathbf{v}_i \times \mathbf{r}_i \Delta t)$ that way like in the conventional method. Instead, we are now able to directly implement the rotation to know the position at $t + \Delta t$, and this is given by

$$\mathbf{r}_i(t + \Delta t) = R_{\hat{\mathbf{v}}_i}(\|\mathbf{v}_i \times \mathbf{r}_i \Delta t\|)\mathbf{r}_i(t), \quad (11)$$

where $R_{\mathbf{n}}(a)$ is the rotation matrix along \mathbf{n} -axis by a . For the construction of $R_{\mathbf{n}}(a)$, one may refer to Euler angles [21]. We adopt Heun's scheme [30] to reduce the artifact caused by discretization with finite Δt .

When $\mathbf{w}_i = 0$, the updated position $\mathbf{r}_i(t + \Delta t)$ by Eq. (11) is on a great circle starting from $\mathbf{r}_i(t)$ because $\mathbf{v}_i \perp \mathbf{r}_i$ for vanishing natural frequency. Therefore, in

this case, the update method Eq. (11) is restored to that suggested in [17]. However, as soon as the natural frequency comes in, the position update does not necessarily take place on a great circle. In general, the new position can be on a various circle, in size and direction, as informed in Eq. (3). Position update as a finite rotation along a proper axis is an inherent feature of the smooth motion on sphere when interpreted for numerical time-mesh Δt . It is hard to tell the dynamically changing rotation axis when the equation of motion is written in the conventional formula Eq. (5).

In analytic point of view, the model equations Eqs. (3) and (5) are same. However, their numerical integration calculated for a finite time-mesh Δt may show a difference depending on the used methods. The new method based on Eq. (3) chases the rotation axis specifying the motion on sphere while the conventional one based on Eq. (5) does not. When the position update by the conventional one is denoted with $\mathbf{r}_c(t + \Delta t)$, the discrepancy from the new method [Eq. (11)] is assessed as $\mathbf{r}(t + \Delta t) = \mathbf{r}_c(t + \Delta t) + \mathcal{O}(\Delta t^2)$ provided $\mathbf{r}(t) = \mathbf{r}_c(t)$. The discrepancy $\mathcal{O}(\Delta t^2)$ comes from the ambiguity of the rotation axis in the conventional method. This asymptotic behavior is readily arguable in Fig. 5 focusing on the geometrical condition among the three objects at the starting point of the black bold arrow.

Above-mentioned discrepancy of $\mathcal{O}(\Delta t^2)$ informs that a numerical scheme of accuracy finer than second order in Δt is required to overcome the ambiguity in rotation axis of the conventional method. For example, the Runge-Kutta 3rd order scheme [30] is at least required for the conventional method. Compared to this, the efficient Heun's scheme basically a case of Runge-Kutta 2nd order scheme is allowed to the new method Eq. (11) equipped with the rotation axis. We remark that, when the discrepancy is not properly reduced, the conventional method could bring about the limited or unreliable numerical realizations of the generic properties of the model, and this again results in the unclear

interpretation on the numerical observations.

In this work, we mainly focus on the near-full synchronization of $\|\mathbf{r}_{\text{CM}}\| \approx 1$ for parallel natural frequency or for strong coupling. But, the other states that do not necessarily show $\|\mathbf{r}_{\text{CM}}\| \approx 1$ are expected for general natural frequency and coupling. However, for this general setting, it is hard to argue the results in an analytic or intuitive way. In this situation, a solid, practical, and reliable numerical method is necessary as an indispensable research methodology. We expect that the new numerical integration method encapsulated in Eq. (11) will play this important role in a competitive way.

VI. SUMMARY

In this paper, we have demonstrated that the standard Kuramoto model can be transformed to the vector product form. This naturally leads to a generalization of the model for the dynamics of 3-dimensional spatial coordinate of agent on unit sphere or, equivalently, that of 2-dimensional spherical phase. Long-term states of the model are surveyed with the geometrical meaning of the vector product form, and the theoretical prediction is numerically supported. We remark that the numerical integration method proposed in the beginning of this field shows an ambiguity when natural frequency is taken into account in the model. A new numerical method free from such ambiguity is illustrated as a direct utilization of our model equation that is composed of vector products in a compact and informative form.

VII. ACKNOWLEDGMENTS

This research was supported by the NRF Grant No. 2018R1D1A1B07049254 (H.K.L.) and 2021R1A2B5B01001951 (H.H.).

-
- [1] Y. Kuramoto, in International Symposium on Mathematical Problems in Theoretical Physics, edited by H. Araki, Lecture Notes on Physics, **30** (Springer, New York, 1975), p.420; *Chemical Oscillations, Waves, and Turbulence* (Springer, Berlin, 1984).
 - [2] S. H. Strogatz, *Physica D* **143**, 1 (2000); *Sync* (Hyperion, New York, 2000).
 - [3] A. Pikovsky, M. Rosenblum, and J. Kurths, *Synchronization: A universal Concept in Nonlinear Sciences* (Cambridge University Press, 2003).
 - [4] J. A. Acebron, L. L. Bonilla, C. J. Perez Vicente, F. Ritort, and R. Spigler, *Rev. Mod. Phys.* **77**, 137 (2005).
 - [5] M. Y. Choi, H. J. Kim, D. Kim, and H. Hong, *Phys. Rev. E* **61**, 371 (2000).
 - [6] J. A. Acebron, L. L. Bonilla, and R. Spigler, *Phys. Rev. E* **62**, 3437 (2000).
 - [7] H. Hong, M. Y. Choi, J. Yi, and K.-S. Soh, *Phys. Rev. E* **59**, 353 (1999).
 - [8] H. Hong, M. Y. Choi, B. G. Yoon, K. Park, and K. S. Soh, *J. Phys. A* **32**, L9 (1999).
 - [9] M. Iwasa and D. Tanaka, *Phys. Rev. E* **81**, 066214 (2010).
 - [10] K. P. O'Keefe, H. Hong, and S. H. Strogatz, *Nature Comm.* **8** 1504 (2017).
 - [11] K. P. O'Keefe and C. Bettstetter, A review of swarmalators and their potential in bio-inspired computing, in *Proc. SPIE 10982, Micro- and Nanotechnology Sensors, Systems, and Applications XI* (2019) p. 10982.
 - [12] H. K. Lee, K. Yeo, and H. Hong, *Chaos* **31**, 033134 (2021).
 - [13] H. Hong, K. Yeo, and H. K. Lee, *Phys. Rev. E* **104**, 044214 (2021).
 - [14] A. Baris and C. Bettstetter, *IEEE Access* **8**, 218752 (2020).

- [15] D. Levis, I. Pagonabarraga, and B. Liebchen, *Phys. Rev. Research* **1**, 023026 (2019).
- [16] D. Escaff and R. Delpiano, *Chaos* **30**, 083137 (2020).
- [17] R. Olfati-Saber, *Swarms on Sphere: A Programmable Swarm with Synchronous Behaviors like Oscillator Networks*, in *Proc. 45th IEEE Conference on Decision and Control* (2006) p. 5060.
- [18] M. A. Lohe, *J. Phys. A: Math. Theor.* **42**, 395101 (2009).
- [19] W.-K. Tung, *Group Theory in Physics* (World Scientific, New Jersey, 1985).
- [20] J. J. Sakurai, *Modern Quantum Mechanics* (Addison-Wesley, Massachusetts, 1994).
- [21] G. B. Arfken and H. J. Weber, *Mathematical Methods for Physicists*, 6th ed. (Elsevier, Amsterdam, 2005).
- [22] M.A. Lohe, *J. Phys. A: Math. Theor.* **43**, 465301 (2010).
- [23] J. Zhu, *Phys. Lett. A* **377**, 2939 (2013).
- [24] D. Chi, S.-H. Choi, and S.-Y. Ha, *J. Math. Phys.* **55**, 052703 (2014).
- [25] S.-H. Choi and S.-Y. Ha, *J. Nonlinear Sci.* **25**, 1257 (2015).
- [26] M.A. Lohe, *J. Phys. A: Math. Theor.* **51**, 225101 (2018).
- [27] J. Markdahl, J. Thunberg, and J. Goncalves, *Automatica* **113**, 108736 (2020).
- [28] M. Lipton, R. Mirolo, and S. H. Strogatz, *Chaos* **31**, 093113 (2021).
- [29] H. Goldstein, *Classical Mechanics*, 2nd ed. (Addison-Wesley, Massachusetts, 1980).
- [30] W. H. Press, S. A. Teukolsky, W. T. Vetterling, and B. P. Flannery, *Numerical Recipes in C*, 2nd ed. (Cambridge University Press, Cambridge, 1992).